



Proposal for suppressing the ac Stark shift in the $\text{He}(2^3S_1 \rightarrow 3^3S_1)$ two-photon transition using magic wavelengths

Yong-Hui Zhang , Li-Yan Tang , and Ting-Yun Shi

State Key Laboratory of Magnetic Resonance and Atomic and Molecular Physics, Wuhan Institute of Physics and Mathematics, Innovation Academy for Precision Measurement Science and Technology, Chinese Academy of Sciences, Wuhan 430071, People's Republic of China



(Received 29 June 2021; accepted 11 October 2021; published 25 October 2021)

Motivated by recent direct measurement of the forbidden $2^3S_1 \rightarrow 3^3S_1$ transition in helium [Thomas *et al.*, *Phys. Rev. Lett.* **125**, 013002 (2020)], where the ac Stark shift is one of the main systematic uncertainties, we propose a dichroic two-photon transition measurement for $2^3S_1 \rightarrow 3^3S_1$, which could effectively suppress the ac Stark shift by utilizing magic wavelengths: one magic wavelength is used to realize state-insensitive optical trapping; the other magic wavelength is used as one of the two lasers driving the two-photon transition. Carrying out calculations based on the no-pair Dirac-Coulomb-Breit Hamiltonian with mass shift operator included, we report the magic wavelength of 1265.615 9(4) nm for ^4He [or 1265.683 9(2) nm for ^3He] can be used to design an optical dipole trap; the magic wavelength of 934.234 5(2) nm for ^4He [or 934.255 4(4) nm for ^3He] can be as one excitation laser in the two-photon process and the ac Stark shift can be reduced to less than 100 kHz, as long as the intensity of the other excitation laser does not exceed $1 \times 10^4 \text{ W/cm}^2$. Alternatively, by selecting detuning frequencies relative to the 2^3P state in the region of 82–103 THz, as well as adjusting the intensity ratios of the two lasers, the ac Stark shift in the $2^3S_1 \rightarrow 3^3S_1$ two-photon transition can be canceled.

DOI: [10.1103/PhysRevA.104.042817](https://doi.org/10.1103/PhysRevA.104.042817)

I. INTRODUCTION

High-precision absolute frequency measurements in helium provide an ideal platform for testing QED theory and determining fundamental constants, such as the fine-structure constant and nuclear charge radius [1–8], which benefits from the abundant laser accessible transition spectra of helium itself. Table I summarizes four transitions from the long-lived metastable 2^3S_1 state to other excited states in ^4He . It is seen that the most precise frequency measurement of helium has reached ppt (10^{-12}) level [8] for the $2^3S_1 \rightarrow 2^1S_0$ transition. Compared with the other three transitions, the uncertainty of 5 MHz [9] for the transition frequency of an ultraweak $2^3S_1 \rightarrow 3^3S_1$ transition in ^4He , which has been measured by single-photon transition, could be further reduced. One of the main systematic uncertainties is due to the ac Stark shift caused by the probe beam with a laser intensity at the focus of $3.86 \times 10^3 \text{ W/cm}^2$, that is 6.9 MHz (exceeds the natural linewidth of 4.43 MHz) [10]. In order to improve the measured precision for the $2^3S_1 \rightarrow 3^3S_1$ transition, suppressing the ac Stark shift effectively becomes a major task in the future experiment.

Reducing the ac Stark shift in a single-photon process for the $2^3S_1 \rightarrow 3^3S_1$ transition might be challenging. The probe laser wavelength 427.7 nm [9] has exceeded the wavelength 663.4 nm of the 3^3S_1 state ionization energy, which will cause the ionization and decrease the population distribution of the 3^3S_1 state. Correspondingly, the detection efficiency of this transition would be affected. We can reduce the frequencies of probe beams through a two-photon process to avoid the ionization, and the ac Stark shift in two-photon transitions can be

suppressed by utilizing two lasers with different wavelengths λ_1 and λ_2 , which has been described and realized in rubidium [12–15], antiproton helium [16,17], and molecular hydrogen ion [18,19]. In the present work of helium, we further propose one of the two lasers (λ_2 laser) is set to be a magic wavelength, at which the 2^3S_1 and 3^3S_1 states have the same dynamic polarizability; then we can minimize the total ac Stark shift in the $2^3S_1 \rightarrow 3^3S_1$ two-photon transition only by carefully controlling the intensity of the λ_1 laser.

Furthermore, the single-photon process for the $2^3S_1 \rightarrow 3^3S_1$ transition, which is excited via the magnetic dipole ($M1$) interaction, is an ultraweak transition since the Einstein A coefficient is at the level of 10^{-9} to 10^{-8} s^{-1} [9,20,21]. The ultraweak transitions can be detected in an optical dipole trap (ODT); moreover, systematic uncertainties can be simultaneously reduced and characterized to the kHz level [11,22]. For example, the most accurate measurement of the ^4He double forbidden $2^3S_1 \rightarrow 2^1S_0$ transition so far benefits from the use of a magic wavelength ODT [8,23]. Based on this, we would also expect to probe the $2^3S_1 \rightarrow 3^3S_1$ two-photon transition in an ODT, preferably operated at a magic wavelength. On the one hand, the lowest-order ac Stark shift of the trapping laser can be canceled; on the other hand, it is helpful to reduce the Doppler shift in the two-photon process.

In this work, for the $2^3S_1 \rightarrow 3^3S_1$ transition spectral measurement, we propose to use a magic wavelength ODT to trap helium atoms, and use two different-wavelength lasers to realize the two-photon excitation with one of them set to be a magic wavelength. To validate the feasibility of the present scheme, the required laser power for trapping helium atoms and the scattering rate limiting the transition coherence

TABLE I. Lifetime of the upper state τ_u , the theoretical natural linewidth Γ , the transition type, the transition rate A , and the current experimental measurement precision for four transitions from the 2^3S_1 state of ^4He .

Transitions	τ_u [10]	Γ	Type	A (s^{-1})	Uncertainty
$2^3S_1 \rightarrow 2^3P$	97.9 ns	1.63 MHz	$E1$	10^7	1.4 kHz [7]
$2^3S_1 \rightarrow 2^1S_0$	20 ms	7.96 Hz	$M1$	6.1×10^{-8}	0.2 kHz [8]
$2^3S_1 \rightarrow 2^1P_1$	0.56 ns	287 MHz	$E1$	1.442	0.5 MHz [11]
$2^3S_1 \rightarrow 3^3S_1$	35.9 ns	4.43 MHz	$M1$	6.48×10^{-9}	5 MHz [9]

lifetime are evaluated; the ac Stark shift is analyzed by controlling the intensity of λ_1 when λ_2 is a magic wavelength. We find that the ac Stark shift in the $2^3S_1 \rightarrow 3^3S_1$ two-photon transition can be suppressed to less than 100 kHz, which paves the way for improving the measured precision of the $2^3S_1 \rightarrow 3^3S_1$ transition frequency. We also find that, with appropriate detuning frequencies, the ac Stark shift in the $2^3S_1 \rightarrow 3^3S_1$ two-photon transition can be minimized to zero by adjusting the laser intensity ratios. Atomic units (a.u.) are used throughout this paper unless stated otherwise.

II. DETAILS OF THE CALCULATIONS

The relativistic energies and wave functions of helium are obtained using the B -spline relativistic configuration interaction (RCI) method that has been described in our previous papers [24–26]. The RCI calculations are carried out by solving the eigenvalue problem of the no-pair Dirac-Coulomb-Breit (DCB) Hamiltonian with mass shift (MS) operator included. The two-electron configuration-state functions are constructed by the positive-energy single-electron wave functions with the orbital angular momenta less than the maximum partial wave ℓ_{max} . The single-electron wave functions are acquired by solving the Dirac equation using Notre Dame basis sets of N B -spline functions of order $k = 7$ [27,28]. The nuclear mass m_0 of ^4He and ^3He are respectively $m_0 = 7294.299\,5361m_e$ and $m_0 = 5495.885\,2754m_e$ [29], where m_e is the electron mass.

Magic wavelengths are located by calculating the dynamic dipole polarizabilities of two states involved in the atomic transition and finding their crossing points. The dynamic dipole polarizability of the magnetic sublevel $|N_g J_g M_g\rangle$ under the linear polarized light with laser frequency ω is given by [25,30,31]

$$\alpha_1(\omega) = \alpha_1^S(\omega) + \frac{3M_g^2 - J_g(J_g + 1)}{J_g(2J_g - 1)}\alpha_1^T(\omega), \quad (1)$$

where the scalar dipole polarizability $\alpha_1^S(\omega)$ is written as

$$\alpha_1^S(\omega) = \sum_{n \neq g} \frac{2|\langle N_g J_g \| T^{(1)} \| N_n J_n \rangle|^2 \Delta E_{gn}}{3(2J_g + 1)(\Delta E_{gn}^2 - \omega^2)}, \quad (2)$$

and the tensor dipole polarizability $\alpha_1^T(\omega)$ is defined as

$$\alpha_1^T(\omega) = \sum_{n \neq g} (-1)^{J_g + J_n} \sqrt{\frac{30(2J_g + 1)J_g(2J_g - 1)}{(2J_g + 3)(J_g + 1)}} \times \begin{Bmatrix} 1 & 1 & 2 \\ J_g & J_g & J_n \end{Bmatrix} \frac{2|\langle N_g J_g \| T^{(1)} \| N_n J_n \rangle|^2 \Delta E_{gn}}{3(2J_g + 1)(\Delta E_{gn}^2 - \omega^2)}, \quad (3)$$

with $\Delta E_{gn} = E_n - E_g$ being the transition energy between the initial state $|N_g J_g\rangle$ and the intermediate state $|N_n J_n\rangle$ and $T^{(1)} = \sum_{i=1}^2 r_i C^{(1)}(\hat{r}_i)$ being the electric dipole transition operator in the length gauge.

The potential depth U of an ODT and the scattering rate Γ_{sc} of atoms can be written in terms of the dynamic dipole polarizability $\alpha_1(\omega)$ [23,32,33],

$$U = \frac{1}{\epsilon_0 c_0} \alpha_1(\omega) \frac{2P}{\pi w_0^2}, \quad (4)$$

$$\Gamma_{sc} = \frac{4}{3h\epsilon_0^2 c_0^4} \omega^3 \alpha_1^2(\omega) I_0, \quad (5)$$

where ϵ_0 , c_0 , and h are the dielectric constant, the speed of light in vacuum, and the Planck constant, respectively, P is the power of the trapping laser beam, w_0 is the beam waist, $I_0 = 2P/(\pi w_0^2)$ is the laser intensity, and ω is the angular frequency of the trapping light. For a magic wavelength ODT, ω is the magic frequency. The physical quantities in Eqs. (4) and (5) are in the International System of Units (SI).

The two-photon electric dipole ($2E1$) differential decay rate of the upper state $|e\rangle$ (or $|N_e J_e M_e\rangle$) to the lower state $|g\rangle$ is given by [34–36]

$$\frac{dA^{2E1}}{d\omega_1} = \frac{8}{9\pi} \alpha^6 \omega_1^3 \omega_2^3 \sum_{q_1 q_2} |M_{q_1 q_2}^{2E1}|^2, \quad (6)$$

where $\alpha = 1/137.035\,999\,074$ [29] is the fine-structure constant, the photon frequencies obey energy conservation, $\omega_1 + \omega_2 = E_e - E_g$, and the two-photon transition matrix element $M_{q_1 q_2}^{2E1}$ can be expressed as

$$M_{q_1 q_2}^{2E1} = \sum_n \left[\frac{\langle e | T_{q_2}^{(1)} | n \rangle \langle n | T_{q_1}^{(1)} | g \rangle}{E_n + \omega_2 - E_e} + \frac{\langle e | T_{q_1}^{(1)} | n \rangle \langle n | T_{q_2}^{(1)} | g \rangle}{E_n + \omega_1 - E_e} \right], \quad (7)$$

with $|n\rangle$ designating intermediate states and $T_{q_i}^{(1)}$ ($i = 1, 2$) being the q_i th component of the electric dipole transition operator. Using the Wigner-Eckart theorem, we perform summations over q_1 , q_2 and magnetic quantum numbers of M_g and M_e ; then we obtain the following expression for the square of transition amplitude $|M^{2E1}|^2$:

$$|M^{2E1}|^2 = \sum_{nn'J} \frac{1}{2J+1} [T_{nJ}(\omega_2) T_{n'J}(\omega_2) + T_{nJ}(\omega_1) T_{n'J}(\omega_1)] + 2 \sum_{nJ_n} \sum_{n'J_{n'}} \begin{Bmatrix} J_{n'} & 1 & J_e \\ J_n & 1 & J_g \end{Bmatrix} (-1)^{J_n + J_{n'}} T_{nJ_n}(\omega_2) \times T_{n'J_{n'}}(\omega_1), \quad (8)$$

TABLE II. Convergence of the scalar and tensor components (in a.u.), $\alpha_1^S(0)$ and $\alpha_1^T(0)$, and the total static dipole polarizabilities (in a.u.) of $\alpha_1(0)(M=0)$ and $\alpha_1(0)(M=\pm 1)$ for the 3^3S_1 state in ^4He and ^3He from RCI calculations. The numbers in parentheses are numerical convergence uncertainties.

(ℓ_{\max}, N)	$\alpha_1^S(0)$	$\alpha_1^T(0)$	$\alpha_1(0)(M=0)$	$\alpha_1(0)(M=\pm 1)$
^4He				
(9, 40)	7940.358 781	0.097 359	7940.164 062	7940.456 142
(10, 40)	7940.361 519	0.097 352	7940.166 815	7940.458 872
(10, 50)	7940.359 702	0.097 547	7940.164 608	7940.457 249
Extrap.	7940.361(4)	0.097(2)	7940.166(4)	7940.458(4)
^3He				
(9, 40)	7942.117 552	0.097 502	7941.922 548	7942.215 054
(10, 40)	7942.120 509	0.097 304	7941.925 900	7942.217 814
(10, 50)	7942.120 877	0.097 174	7941.926 530	7942.218 051
Extrap.	7942.121(6)	0.097(2)	7941.927(8)	7942.218(6)

where

$$T_{nJ_n}(\omega) = \frac{\langle N_e J_e \| T^{(1)} \| N_n J_n \rangle \langle N_n J_n \| T^{(1)} \| N_g J_g \rangle}{E_n + \omega - E_e}. \quad (9)$$

III. RESULTS AND DISCUSSIONS

A. Dipole polarizabilities

We use a complete set of configuration wave functions on an exponential grid [37] generated using B splines constrained to a spherical cavity. A cavity radius of 200 a.u. is chosen to accommodate the initial state and the corresponding intermediate states, and it is also suitable for obtaining dynamic dipole polarizabilities of the 2^3S_1 and 3^3S_1 states for $\omega < 0.068$ a.u., which corresponds to the ionization energy of the $\text{He}(3^3S_1)$ state. The basis set consists of $N = 40, 45,$ and 50 splines for each value of the partial wave that is less than $\ell_{\max} = 10$. The numerical uncertainty is evaluated by doubling the maximum difference between the extrapolated value and those given in the last three larger basis sets of convergence tables.

As the numbers of the partial wave and B splines increased, the convergence studies for the scalar and tensor polarizabilities, $\alpha_1^S(0)$ and $\alpha_1^T(0)$, and the static dipole polarizabilities of $\alpha_1(0)(M=0)$ and $\alpha_1(0)(M=\pm 1)$ for the 3^3S_1 state in ^4He and ^3He are presented in Table II. For ^4He , the present RCI value of $\alpha_1^S(0)$ is 7940.361(4) a.u. with six convergent figures. Compared with the static polarizability of 7937.58(1) a.u. [38] for $^\infty\text{He}$, it indicates that the static dipole polarizability is increased by 2.78 a.u. due to the finite nuclear mass and relativistic effects. These effects on ^3He are more obvious than ^4He .

B. Determination of magic wavelengths

The magic wavelengths for the $2^3S_1 \rightarrow 3^3S_1$ transitions need to be determined separately for the $M=0$ and $M=\pm 1$ cases, since the total dynamic dipole polarizabilities for the 2^3S_1 and 3^3S_1 states depend upon the magnetic quantum numbers M . Figure 1 is the dynamic dipole polarizability in the range of 770–1300 nm for the $2^3S_1(M=\pm 1)$ and $3^3S_1(M=0)$ magnetic sublevels of ^4He . There are five

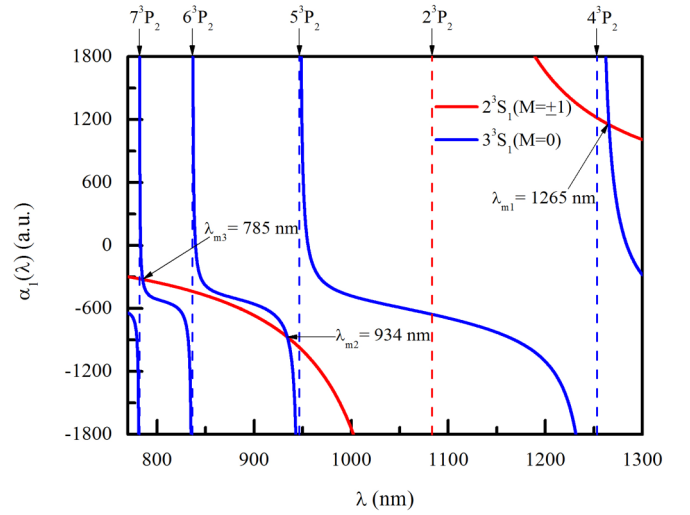


FIG. 1. Dynamic dipole polarizabilities for the $2^3S_1(M=\pm 1)$ and $3^3S_1(M=0)$ states of ^4He . The magic wavelengths are marked with arrows. The positions of the resonances are indicated by vertical dashed lines with small arrows on top of the graph.

resonances ($2^3S_1 \rightarrow 2^3P_2$, $3^3S_1 \rightarrow 4^3P_2$, $3^3S_1 \rightarrow 5^3P_2$, $3^3S_1 \rightarrow 6^3P_2$, and $3^3S_1 \rightarrow 7^3P_2$) existing in this wavelength region, which are indicated by vertical dashed lines with small arrows on top of the graph. Three magic wavelengths of λ_{m1} , λ_{m2} , and λ_{m3} around 1265, 934, and 785 nm for the $2^3S_1(M=\pm 1) \rightarrow 3^3S_1(M=0)$ transition are all marked with arrows in Fig. 1.

In previous work [39], the magic wavelengths for the $2^3S \rightarrow 3^3S$ transition of $^\infty\text{He}$ have been determined based on NRCI calculations. In the present RCI calculations, we take account of the finite nuclear mass and relativistic effects on magic wavelengths and dynamic dipole polarizabilities. The updated results of ^4He and ^3He are shown in Table III.

Furthermore, for ^3He , we consider the hyperfine interactions on magic wavelengths and polarizabilities. The dipole matrix elements between different hyperfine levels are transformed from the present matrix elements using the Wigner-Eckart theorem [40]. The hyperfine energy shifts given in Table 7 of Ref. [41] are added to the present RCI energies of 2^3S_1 , 3^3S_1 , and $n^{1,3}P_{1,2,3}$ ($n \leq 10$) to obtain the corresponding hyperfine energies. The dynamic polarizabilities for different hyperfine magnetic sublevels $|FM_F\rangle$ are calculated using Eqs. (1)–(3) by replacing J and M with F and M_F , respectively. Then polarizabilities and magic wavelengths for different hyperfine transitions can be determined. Table IV shows magic wavelengths and the corresponding dynamic polarizabilities for different hyperfine transitions of ^3He . Compared with the RCI calculated results of Table III, it is seen that magic wavelengths become shorter due to the hyperfine interactions, and the dynamic dipole polarizabilities at the corresponding magic wavelengths are increased.

C. 1265 nm magic wavelength to design an ODT

The magic wavelength with a positive dynamic dipole polarizability can be used to design an ODT referring to Eq. (4). From Tables III and IV, it is seen that, among the magic

TABLE III. Magic wavelengths (in nm) and the corresponding dynamic dipole polarizabilities (in a.u.) obtained from RCI calculations for the $2^3S_1 \rightarrow 3^3S_1$ transition of ^4He and ^3He , and the numbers in parentheses are numerical convergence uncertainties. For each transition, the first line refers to ^4He and the second line to ^3He .

Transition	λ_{m1}	$\alpha_1(\lambda_{m1})$	λ_{m2}	$\alpha_1(\lambda_{m2})$	λ_{m3}	$\alpha_1(\lambda_{m3})$
$2^3S_1(M=0) \rightarrow 3^3S_1(M=0)$	1265.617 5(2)	1151.339(4)	934.243 5(2)	-872.234(6)	785.327 4(2)	-324.405(2)
	1265.691 6(2)	1151.954(6)	934.270 1(6)	-871.75(2)	785.366(2)	-324.363(2)
$2^3S_1(M=0) \rightarrow 3^3S_1(M=\pm 1)$	1265.625 8(2)	1151.298(4)	934.245 0(2)	-872.245(6)	785.329 5(2)	-324.409(2)
	1265.699 9(2)	1151.913(6)	934.271 6(6)	-871.76(2)	785.369(2)	-324.366(2)
$2^3S_1(M=\pm 1) \rightarrow 3^3S_1(M=0)$	1265.615 9(4)	1151.590(4)	934.234 5(2)	-871.951(4)	785.326 8(2)	-324.362(2)
	1265.689 9(2)	1152.205(6)	934.261 2(4)	-871.47(2)	785.366(2)	-324.320(2)
$2^3S_1(M=\pm 1) \rightarrow 3^3S_1(M=\pm 1)$	1265.624 2(2)	1151.549(4)	934.236 0(2)	-871.962(4)	785.328 8(2)	-324.366(2)
	1265.698 2(2)	1152.164(6)	934.262 7(4)	-871.48(2)	785.368(2)	-324.323(2)

wavelengths λ_{m1} , λ_{m2} , and λ_{m3} , only the dynamic polarizability at the magic wavelength around 1265 nm is positive. Including the finite nuclear mass and relativistic effects, the results of this particular magic wavelength are given to be 1265.615 9(4) nm for the $2^3S_1(M=\pm 1) \rightarrow 3^3S_1(M=0)$ transition of ^4He and 1265.683 9(2) nm for the $2^3S_1(F=3/2, M_F=\pm 3/2) \rightarrow 3^3S_1(F=3/2, M_F=\pm 1/2)$ hyperfine transition of ^3He . The corresponding dynamic dipole polarizabilities for ^4He and ^3He are 1151.590(4) and 1152.221(6) a.u., respectively. These large dynamic dipole polarizabilities indicate that the magic wavelength around 1265 nm might be useful for the design of an ODT with further analysis.

On the one hand, the design of an ODT needs enough depth to capture a certain number of atoms. Generally, a natural scale for the minimum depth of an optical trap as required for efficient loading is set to be a few $10T_r$, where $T_r = 2E_r$ is the recoil temperature and $E_r = h^2/2m\lambda_m^2$ is the photon recoil energy [32]. The larger the photon recoil energy, the deeper the trap depth and the higher the laser power required. The photon recoil energy at the 1265 nm magic wavelength is calculated to be $E_r = 1.493 \mu\text{K}$ for ^4He and $1.982 \mu\text{K}$ for ^3He . Supposing the trap depth to be as low as $20E_r$, to obtain the required laser power for creating this supposed trap depth conservatively, the focused laser beam with a large beam waist of $100 \mu\text{m}$ is needed. According to Eq. (4), we obtain the required laser powers for different transitions, that are listed in the second to the last line of Table V. The required laser powers are about 0.9 W for ^4He and 1.2 W for ^3He , which are feasible under current advanced laser technology. Therefore, we believe that, for the $2^3S_1 \rightarrow 3^3S_1$ transition, using the magic wavelength at 1265 nm with the laser power around 1 W can create a trap depth of about $30 \mu\text{K}$ for ^4He and $40 \mu\text{K}$ for ^3He .

On the other hand, the design of an ODT needs a small atomic scattering rate, since the low scattering rate ensures enough time for exciting the He atom from the 2^3S_1 state to the 3^3S_1 state. Using the calculated trapping beam power P that can create the supposed $20E_r$ deep trap, we estimate the scattering rates for ^4He and ^3He isotopes at the magic wavelength around 1265 nm; then the trapping lifetimes are also obtained, which are given in the last line of Table V. The trapping lifetimes are about 4.6 s for ^4He and 3.5 s for ^3He , which are long enough to perform spectral measurement of the forbidden $2^3S_1 \rightarrow 3^3S_1$ transition.

D. Suppressing ac Stark shift in two-photon transition

It is seen from Sec. III C that, once we use the laser with the magic wavelength around 1265 nm to build an ODT, the ac Stark shift in the $2^3S_1 \rightarrow 3^3S_1$ transition caused by the trapping beam can be minimized to zero. However, the ac Stark shift caused by the probe laser has become the focus in the spectroscopy measurement of the $2^3S_1 \rightarrow 3^3S_1$ transition. In this subsection, we will propose a two-photon excitation scheme to suppress the ac Stark shift in the probing process. The two-photon transition of $2^3S_1 \rightarrow 3^3S_1$ in ^4He is shown graphically in Fig. 2. This two-photon transition is excited by two different lasers with wavelengths of λ_1 and λ_2 . The detuning frequency of $\Delta\omega_d$ indicates the relative position of the virtual state to the real 2^3P state.

To discuss the feasibility of the proposed scheme mentioned above, we first calculate the two-photon transition amplitudes at different detuning frequencies. Figure 3 plots the transition amplitudes $|M^{2E1}|$ of the $2^3S_1 \rightarrow 3^3S_1$ two-photon transition in ^4He at different detuning frequencies $\Delta\omega_d$, and several selected values of $|M^{2E1}|$ are listed in Table VI. As seen from Fig. 3, the curve of $|M^{2E1}|$ is symmetric with respect to $\Delta\omega_d = 73.73 \text{ THz}$, corresponding to a

TABLE IV. Magic wavelengths (in nm) and the corresponding dynamic polarizabilities (in a.u.) for the hyperfine transition of $2^3S_1, F=3/2, \rightarrow 3^3S_1, F=3/2$ of ^3He . The numbers in parentheses are numerical convergence uncertainties.

Transition	λ_{m1}	$\alpha_1(\lambda_{m1})$	λ_{m2}	$\alpha_1(\lambda_{m2})$	λ_{m3}	$\alpha_1(\lambda_{m3})$
$2^3S_1(M_F=\pm 1/2) \rightarrow 3^3S_1(M_F=\pm 1/2)$	1265.685 1(2)	1152.037(6)	934.261 9(4)	-871.65(2)	785.363(2)	-324.347(2)
$2^3S_1(M_F=\pm 1/2) \rightarrow 3^3S_1(M_F=\pm 3/2)$	1265.682 0(2)	1152.053(8)	934.256 8(6)	-871.61(2)	785.361(2)	-324.343(2)
$2^3S_1(M_F=\pm 3/2) \rightarrow 3^3S_1(M_F=\pm 1/2)$	1265.683 9(2)	1152.221(6)	934.255 4(4)	-871.44(2)	785.362(2)	-324.316(2)
$2^3S_1(M_F=\pm 3/2) \rightarrow 3^3S_1(M_F=\pm 3/2)$	1265.680 7(2)	1152.236(6)	934.250 3(6)	-871.40(2)	785.361(2)	-324.312(2)

TABLE V. 1265 nm magic wavelengths of ${}^4\text{He}$ ($2^3S_1, M = \pm 1 \rightarrow 3^3S_1, M = 0$) and ${}^3\text{He}$ ($2^3S_1, F = 3/2, M_F = \pm 3/2 \rightarrow 3^3S_1, F = 3/2, M_F = \pm 1/2$), dynamic dipole polarizabilities, and the photon recoil energies for ${}^4\text{He}$ and ${}^3\text{He}$. Supposing that a $20E_r$ trapping depth is created and the focused laser has a beam waist of $100 \mu\text{m}$, the required laser beam power P and the corresponding trapping lifetime $\tau_{sc} = 1/\Gamma_{sc}$ are given in the last two lines. The numbers in parentheses are numerical convergence uncertainties.

	Units	${}^4\text{He}$	${}^3\text{He}$
λ_m	nm	1265.615 9(4)	1265.683 9(2)
$\alpha_1(\lambda_m)$	a.u.	1151.590(4)	1152.221(6)
E_r	μK	1.493	1.982
P	W	0.905	1.201
τ_{sc}	s	4.596	3.459

conventional single-color case where the two-photon transition absorbs two equal-frequency photons. From this symmetry position, with the decrease (or increase) of $\Delta\omega_d$, i.e., the virtual state is increasingly near to (or far away from) the real 2^3P state, the transition amplitude is enhanced significantly. For $\Delta\omega_d = 42.46$ THz and $\Delta\omega_d = 103.31$ THz marked by magenta diamond and red solid circle, respectively, in Fig. 3, both of the two-photon transition amplitudes are over 1.5×10^3 a.u., which are 192 times larger than the transition amplitude of 7.8 a.u. for the $\text{H}(1s \rightarrow 2s)$ two-photon transition at $\lambda_1 = \lambda_2 = 243$ nm [42]. In addition, the nonresonant two-photon decay rate is estimated to be 0.065 s^{-1} , that is, at least six orders of magnitude larger than the magnetic dipole transition rate [9]. These calculations provide a theoretical support for the feasibility of two-photon spectroscopy measurement of the $\text{He}(2^3S_1 \rightarrow 3^3S_1)$ transition.

We next evaluate the ac Stark shift in the $2^3S_1 \rightarrow 3^3S_1$ two-photon transition. While the two lasers with wavelengths λ_1 and λ_2 drive the two-photon transition, to the leading order in laser intensity and the fine-structure constant, the ac Stark shift can be calculated according to the following formula:

$$\Delta E_{ac} = -\frac{1}{c_0 \epsilon_0} [\Delta\alpha_1(\lambda_1)I_1 + \Delta\alpha_1(\lambda_2)I_2], \quad (10)$$

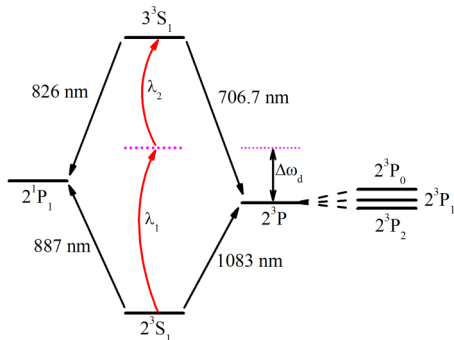


FIG. 2. Energy-level diagram indicating the $2^3S_1 \rightarrow 3^3S_1$ two-photon transition of ${}^4\text{He}$ excited by two lasers with wavelengths of λ_1 and λ_2 . The detuning frequency of $\Delta\omega_d$ represents the relative position of the virtual state to the real 2^3P state. The single-photon transition wavelength of $2^3S_1 \rightarrow 3^3S_1$ is 427.7 nm. Other relevant transition wavelengths are indicated.

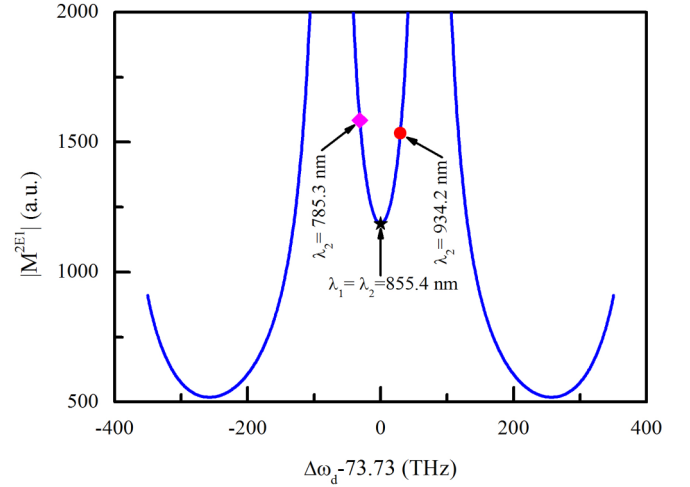


FIG. 3. Transition amplitude $|M^{2E1}|$ of the $2^3S_1 \rightarrow 3^3S_1$ two-photon transition of ${}^4\text{He}$ as a function of the detuning frequency $\Delta\omega_d$. The two-photon transition is excited by two different lasers with wavelengths of λ_1 and λ_2 . Three positions marked by arrows from left to right indicate the cases with $\Delta\omega_d = 42.46$, 73.73 , and 103.31 THz. For $\Delta\omega_d = 42.46$ and 103.31 THz, λ_2 are respectively the 785.3 and 934.2 nm magic wavelengths and, for $\Delta\omega_d = 73.73$ THz, two lasers have equal wavelengths.

where the units are in SI, $\Delta\alpha_1(\lambda_i)$ is the difference of the electric dipole polarizabilities between the $3^3S_1(M = 0)$ and $2^3S_1(M = \pm 1)$ states, and the laser intensity $I_i = c\epsilon_0 F_i^2/2$, with F_i being the electric-field amplitude and $i = 1, 2$. Compared to the $E1$ contribution, the next-order dynamic electric quadrupole ($E2$) and magnetic dipole polarizabilities are respectively suppressed by a factor of $(\alpha\omega)^2$ and a factor of α^2 [33,43], and there are no resonant contributions for the $E2$ and $M1$ polarizabilities at the frequencies of interest, so contributions from other multipole polarizabilities are neglected under the present calculations.

At different detuning frequencies, the laser wavelengths λ_1 and λ_2 exciting the $2^3S_1 \rightarrow 3^3S_1$ two-photon transition and the corresponding differences of dynamic polarizabilities between the $3^3S_1(M = 0)$ and $2^3S_1(M = \pm 1)$ states of ${}^4\text{He}$

TABLE VI. Detuning frequency $\Delta\omega_d$, the two-photon transition amplitudes $|M^{2E1}|$, the laser wavelengths λ_1 and λ_2 exciting the two-photon transition, and the differences of dynamic dipole polarizabilities, $\Delta\alpha_1(\lambda_i)$, between the $3^3S_1(M = 0)$ and $2^3S_1(M = \pm 1)$ states of ${}^4\text{He}$ at different laser wavelengths λ_i , $i = 1, 2$.

$\Delta\omega_d$ (THz)	$ M^{2E1} $ (a.u.)	λ_i (nm)	$\Delta\alpha_1(\lambda_i)$ (a.u.)	
			(λ_1, λ_2)	$\Delta\alpha_1(\lambda_1)$
103.31	1534.0	(788.8, 934.2)	-108.51	0
73.73	1185.7	(855.4, 855.4)	70.45	70.45
42.46	1583.5	(939.2, 785.3)	-220.54	0
100	1450.5	(795.8, 924.4)	-152.99	108.24
10	6347.5	(1045.5, 723.8)	3548.4	-1122.6
1	63 804	(1079.4, 708.4)	4.15×10^4	-1.08×10^4
0.1	6.79×10^5	(1082.9, 706.9)	4.25×10^5	-1.23×10^5
0.01	6.7×10^6	(1083.3, 706.7)	4.8×10^6	-5.46×10^5

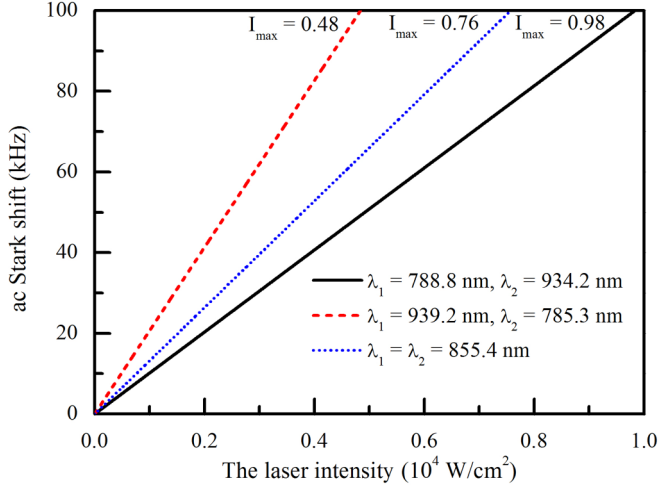


FIG. 4. ac Stark shifts in the $2^3S_1 \rightarrow 3^3S_1$ two-photon transition of ^4He at different intensities of the λ_1 laser. I_{\max} indicates the maximum intensity of the λ_1 laser when the ac Stark shift equals 100 kHz. The two-photon transition is excited by two lasers with wavelengths of λ_1 and λ_2 . The ac Stark shifts are estimated using dynamic dipole polarizabilities of $2^3S_1(M = \pm 1)$ and $3^3S_1(M = 0)$.

are given in Table VI as well. We can see that, with $\Delta\omega_d$ decreasing from 100 THz to 0.01 THz, the difference of polarizabilities between the 3^3S_1 and 2^3S_1 states increases by three to four orders of magnitude, which will result in a large variation of the ac Stark shift in the two-photon transition when $\Delta\omega_d$ varies. For $\Delta\omega_d = 73.73$ THz, the total ac Stark shift will be twice that of the Stark shift in the λ_1 laser field. For $\Delta\omega_d = 42.46$ and 103.31 THz, the total ac Stark shift is only related to the λ_1 laser field, and the ac Stark shift induced by the λ_2 laser will vanish since λ_2 is a magic wavelength given in Sec. III B.

The ac Stark shifts in the $2^3S_1 \rightarrow 3^3S_1$ two-photon transition of ^4He as the λ_1 laser intensity changed are plotted in Fig. 4. The maximum laser intensity I_{\max} is given for suppressing the total ac Stark shift to be 100 kHz. We can see that, to suppress the ac Stark shift at the same level, the laser intensity for $\Delta\omega_d = 103.31$ THz (corresponding to $\lambda_1 = 788.8$ nm and $\lambda_2 = 934.2$ nm) is largest, which will make it easier to drive the two-photon transition. Moreover, for $\Delta\omega_d = 103.31$ THz, as long as the λ_1 laser intensity does not exceed 1×10^4 W/cm², the total ac Stark shift caused by probe beams will be less than 100 kHz, which would be about 70-fold smaller than the single-photon measurement [9]. With this laser intensity, the collision heating caused by the probe beam is about $0.5 \mu\text{K s}^{-1}$, which will not destroy the stability of the ODT. Also the laser intensity within the proposed maximum limit of 1×10^4 W/cm² is high enough to drive the two-photon transition, since the laser intensity in the $2^3S_1 \rightarrow 3^3S_1$ single-photon transition experiment is 3.86×10^3 W/cm² [9] and we mentioned earlier that the two-photon transition rate is much larger than the single-photon M1 transition rate. Therefore, we suggest using these two lasers with wavelengths of $\lambda_1 = 788.8$ nm and $\lambda_2 = 934.2$ nm that

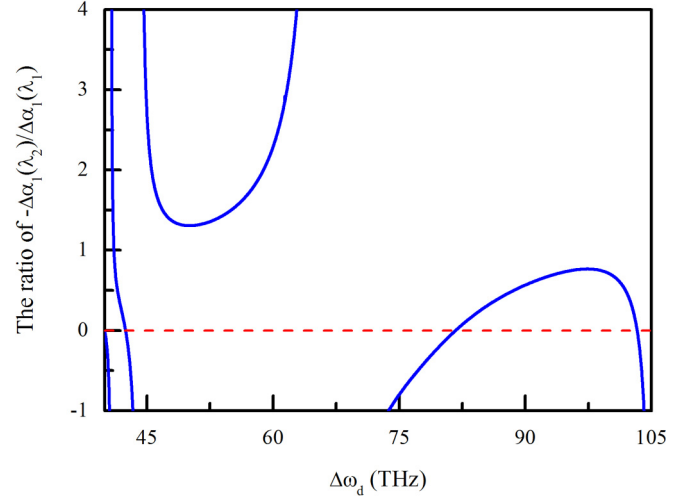


FIG. 5. Ratios of $-\Delta\alpha_1(\lambda_2)/\Delta\alpha_1(\lambda_1)$ at different detuning frequencies $\Delta\omega_d$. $\Delta\alpha_1(\lambda_1)$ and $\Delta\alpha_1(\lambda_2)$ are the differences of polarizabilities between the $3^3S_1(M = 0)$ and $2^3S_1(M = \pm 1)$ states of ^4He at the wavelengths of λ_1 and λ_2 , respectively. The red dashed line is a horizontal zero line.

are also well detuned from electric dipole transition frequencies, to realize the two-photon transition. The values for the λ_2 magic wavelength are 934.234 5(2) nm and 934.255 4(4) nm for $^4\text{He}(2^3S_1, M = \pm 1 \rightarrow 3^3S_1, M = 0)$ and $^3\text{He}(2^3S_1, F = 3/2, M_F = \pm 3/2 \rightarrow 3^3S_1, F = 3/2, M_F = \pm 1/2)$, respectively.

In addition, from Eq. (10) we see that, when $-\Delta\alpha_1(\lambda_2)/\Delta\alpha_1(\lambda_1)$ is a positive value, the ac Stark shift can be canceled by adjusting the laser intensity ratio I_1/I_2 equal to $-\Delta\alpha_1(\lambda_2)/\Delta\alpha_1(\lambda_1)$. Gerginov and Beloy have demonstrated this method on the $5s^2S_{1/2} \rightarrow 5d^2D_{5/2}$ two-photon transition in ^{87}Rb [14]. Considering comprehensively the two-photon transition amplitude and the residual first-order Doppler broadening due to the unequal laser wavelengths, for the $2^3S_1 \rightarrow 3^3S_1$ two-photon transition of helium, the ratios of $-\Delta\alpha_1(\lambda_2)/\Delta\alpha_1(\lambda_1)$ only at $\Delta\omega_d = 40$ –105 THz are shown in Fig. 5. It is seen that, for $\Delta\omega_d$ in the region of 82–103 THz, the ratios are positive and less than one, so the ac Stark shift cancellation method with an appropriate intensity ratio can also be used in the $\text{He}(2^3S_1 \rightarrow 3^3S_1)$ two-photon transition. For example, driving the two-photon transition with the intensity ratio of $I_1/I_2 = 0.707$ will achieve zero ac Stark shift for $\Delta\omega_d = 100$ THz given in Table VI and a 0.1% intensity ratio change leads to a 1.2-fold increase in the total ac Stark shift.

IV. CONCLUSION

We have determined magic wavelengths for the $2^3S_1 \rightarrow 3^3S_1$ forbidden transition in ^4He and ^3He isotopes and proposed an experimental scheme for suppressing the ac Stark shift in the $2^3S_1 \rightarrow 3^3S_1$ transition frequency measurement. For ^4He , the 1265.615 9(4) nm magic wavelength can be used to design an optical dipole trap, which can create a $20E_r$ trap depth with the laser power of 0.9 W and a 4.6 s trapping

lifetime. Furthermore, the 934.234 5(2) nm magic wavelength is suggested as the λ_2 laser to excite the two-photon process for the $2^3S_1 \rightarrow 3^3S_1$ transition, and the ac Stark shift would be reduced to about 70-fold smaller compared to the single-photon transition, as long as the intensity of the λ_1 laser does not exceed 1×10^4 W/cm². Similarly, for ^3He , the 1265.683 9(2) nm magic wavelength can be used to design an ODT and the 934.255 4(4) nm magic wavelength can be as the λ_2 laser to realize the $2^3S_1 \rightarrow 3^3S_1$ two-photon transition process. Alternatively, for detuning frequencies relative to the 2^3P state in the region of 82–103 THz, driving the two-photon transition with appropriate intensity ratios will achieve zero ac Stark shift. We expect that our proposal can improve the measured precision of the $\text{He}(2^3S_1 \rightarrow 3^3S_1)$ transition frequency.

ACKNOWLEDGMENTS

We would like to thank C.-B. Li, L.-Q. Hua, and Y. R. Sun for their helpful comments on the manuscript, and thank Prof. G. W. F. Drake for instructive discussions regarding the two-photon transitions. This work was supported by the National Natural Science Foundation of China under Grants No. 11704398 and No. 11774386, by the Strategic Priority Research Program of the Chinese Academy of Sciences, Grants No. XDB21010400 and No. XDB21030300, by the National Key Research and Development Program of China under Grant No. 2017YFA0304402, and by the Hubei Province Science Fund for Distinguished Young Scholars No. 2019CFA058.

-
- [1] K. Pachucki, V. Patkóš, and V. A. Yerokhin, *Phys. Rev. A* **95**, 062510 (2017).
- [2] V. Patkóš, V. A. Yerokhin, and K. Pachucki, *Phys. Rev. A* **101**, 062516 (2020).
- [3] V. Patkóš, V. A. Yerokhin, and K. Pachucki, *Phys. Rev. A* **103**, 012803 (2021).
- [4] X. Zheng, Y. R. Sun, J. J. Chen, W. Jiang, K. Pachucki, and S. M. Hu, *Phys. Rev. Lett.* **118**, 063001 (2017).
- [5] K. Kato, T. D. G. Skinner, and E. A. Hessels, *Phys. Rev. Lett.* **121**, 143002 (2018).
- [6] P. Cancio Pastor, L. Consolino, G. Giusfredi, P. De Natale, M. Inguscio, V. A. Yerokhin, and K. Pachucki, *Phys. Rev. Lett.* **108**, 143001 (2012).
- [7] X. Zheng, Y. R. Sun, J. J. Chen, W. Jiang, K. Pachucki, and S. M. Hu, *Phys. Rev. Lett.* **119**, 263002 (2017).
- [8] R. J. Rengelink, Y. van der Werf, R. P. M. J. W. Notermans, R. Jannin, K. S. E. Eikema, M. D. Hoogerland, and W. Vassen, *Nat. Phys.* **14**, 1132 (2018).
- [9] K. F. Thomas, J. A. Ross, B. M. Henson, D. K. Shin, K. G. H. Baldwin, S. S. Hodgman, and A. G. Truscott, *Phys. Rev. Lett.* **125**, 013002 (2020).
- [10] W. L. Wiese and J. R. Fuhr, *J. Phys. Chem. Ref. Data* **38**, 565 (2009).
- [11] R. P. M. J. W. Notermans and W. Vassen, *Phys. Rev. Lett.* **112**, 253002 (2014).
- [12] C. Perrella, P. S. Light, J. D. Anstie, T. M. Stace, F. Benabid, and A. N. Luiten, *Phys. Rev. A* **87**, 013818 (2013).
- [13] K. W. Martin, B. Stuhl, J. Eugenio, M. S. Safronova, G. Phelps, J. H. Burke, and N. D. Lemke, *Phys. Rev. A* **100**, 023417 (2019).
- [14] V. Gerginov and K. Beloy, *Phys. Rev. Applied* **10**, 014031 (2018).
- [15] C. Perrella, P. S. Light, J. D. Anstie, F. N. Baynes, R. T. White, and A. N. Luiten, *Phys. Rev. Applied* **12**, 054063 (2019).
- [16] M. Hori and V. I. Korobov, *Phys. Rev. A* **81**, 062508 (2010).
- [17] M. Hori, A. Sótér, D. Barna, A. Dax, R. Hayano, S. Friedreich, B. Juhász, T. Pask, E. Widmann, D. Horváth *et al.*, *Nature (London)* **475**, 484 (2011).
- [18] V. Q. Tran, J. P. Karr, A. Douillet, J. C. J. Koelemeij, and L. Hilico, *Phys. Rev. A* **88**, 033421 (2013).
- [19] S. Patra, M. Germann, J. P. Karr, M. Haidar, L. Hilico, V. I. Korobov, F. Cozijn, K. Eikema, W. Ubachs, and J. C. J. Koelemeij, *Science* **369**, 1238 (2020).
- [20] A. Derevianko, I. M. Savukov, W. R. Johnson, and D. R. Plante, *Phys. Rev. A* **58**, 4453 (1998).
- [21] G. Łach and K. Pachucki, *Phys. Rev. A* **64**, 042510 (2001).
- [22] R. van Rooij, J. S. Borbely, J. Simonet, M. D. Hoogerland, K. S. E. Eikema, R. A. Rozendaal, and W. Vassen, *Science* **333**, 196 (2011).
- [23] R. P. M. J. W. Notermans, R. J. Rengelink, K. A. H. van Leeuwen, and W. Vassen, *Phys. Rev. A* **90**, 052508 (2014).
- [24] Y. H. Zhang, F. F. Wu, P. P. Zhang, L. Y. Tang, J. Y. Zhang, K. G. H. Baldwin, and T. Y. Shi, *Phys. Rev. A* **99**, 040502(R) (2019).
- [25] F. F. Wu, S. J. Yang, Y. H. Zhang, J. Y. Zhang, H. X. Qiao, T. Y. Shi, and L. Y. Tang, *Phys. Rev. A* **98**, 040501(R) (2018).
- [26] Y. H. Zhang, L. Y. Tang, J. Y. Zhang, and T. Y. Shi, *Phys. Rev. A* **103**, 032810 (2021).
- [27] W. R. Johnson, S. A. Blundell, and J. Sapirstein, *Phys. Rev. A* **37**, 307 (1988).
- [28] L. Y. Tang, Y. H. Zhang, X. Z. Zhang, J. Jiang, and J. Mitroy, *Phys. Rev. A* **86**, 012505 (2012).
- [29] P. J. Mohr, B. N. Taylor, and D. B. Newell, *Rev. Mod. Phys.* **84**, 1527 (2012).
- [30] J. Mitroy, M. S. Safronova, and C. W. Clark, *J. Phys. B* **43**, 202001 (2010).
- [31] Y. H. Zhang, L. Y. Tang, X. Z. Zhang, and T. Y. Shi, *Phys. Rev. A* **93**, 052516 (2016).
- [32] R. Grimm, M. Weidemüller, and Y. B. Ovchinnikov, *Adv. At., Mol., Opt. Phys.* **42**, 95 (2000).
- [33] S. G. Porsev, A. Derevianko, and E. N. Fortson, *Phys. Rev. A* **69**, 021403(R) (2004).
- [34] M. S. Safronova, W. R. Johnson, and U. I. Safronova, *J. Phys. B* **43**, 074014 (2010).
- [35] A. Derevianko and W. R. Johnson, *Phys. Rev. A* **56**, 1288 (1997).
- [36] A. T. Bondy, D. C. Morton, and G. W. F. Drake, *Phys. Rev. A* **102**, 052807 (2020).
- [37] H. Bachau, E. Cormier, P. Declève, J. E. Hansen, and F. Martín, *Rep. Prog. Phys.* **64**, 1815 (2001).

- [38] Z. C. Yan, *Phys. Rev. A* **62**, 052502 (2000).
- [39] Y. H. Zhang, L. Y. Tang, X. Z. Zhang, and T. Y. Shi, *Phys. Rev. A* **92**, 012515 (2015).
- [40] J. Jiang and J. Mitroy, *Phys. Rev. A* **88**, 032505 (2013).
- [41] D. C. Morton, Q. Wu, and G. W. F. Drake, *Can. J. Phys.* **84**, 83 (2006).
- [42] M. Haas, U. D. Jentschura, C. H. Keitel, N. Kolachevsky, M. Herrmann, P. Fendel, M. Fischer, T. Udem, R. Holzwarth, T. W. Hänsch, M. O. Scully, and G. S. Agarwal, *Phys. Rev. A* **73**, 052501 (2006).
- [43] S. G. Porsev, M. S. Safronova, U. I. Safronova, and M. G. Kozlov, *Phys. Rev. Lett.* **120**, 063204 (2018).